Supporting Information

"Internal and External Combined" Nonradiative Decay-Based Nanoagent for Photoacoustic Image-Guided Highly Efficient Photothermal Therapy

Hua Gu[†], Weijian Liu[†], Shijie Zhen[‡], Saran Long[†,§], Wen Sun[†,§], Jianfang Cao[//], Xueze Zhao[†], Jianjun Du[†,§], Jiangli Fan[*,†,§], Xiaojun Peng[†]

[†]State Key Laboratory of Fine Chemicals, Dalian University of Technology, Dalian 116024, China. 1

[‡]Guangxi Key Laboratory of Electrochemical and Magneto-chemical Functional Materials, College of Chemistry and Bioengineering, Guilin University of Technology, Guilin 541006, China.

[§]Ningbo Institute of Dalian University of Technology, Ningbo 315016, China

[//]School of Chemical Engineering, Dalian University of Technology, Panjin Campus, Panjin 124221, China

*: Corresponding author. E-mail: fanjl@dlut.edu.cn

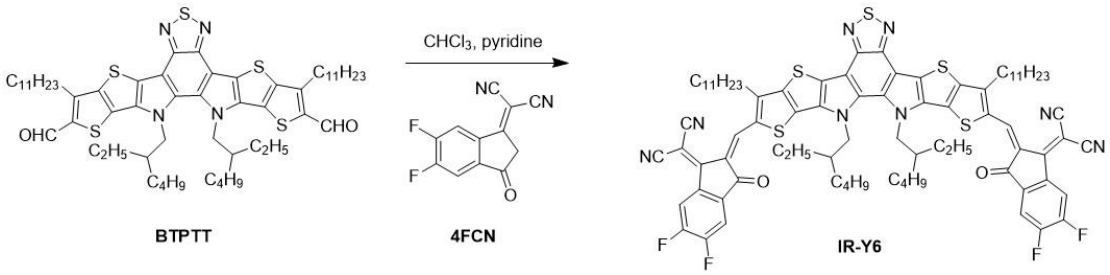

Scheme S1 Synthetic route of IR-Y6.

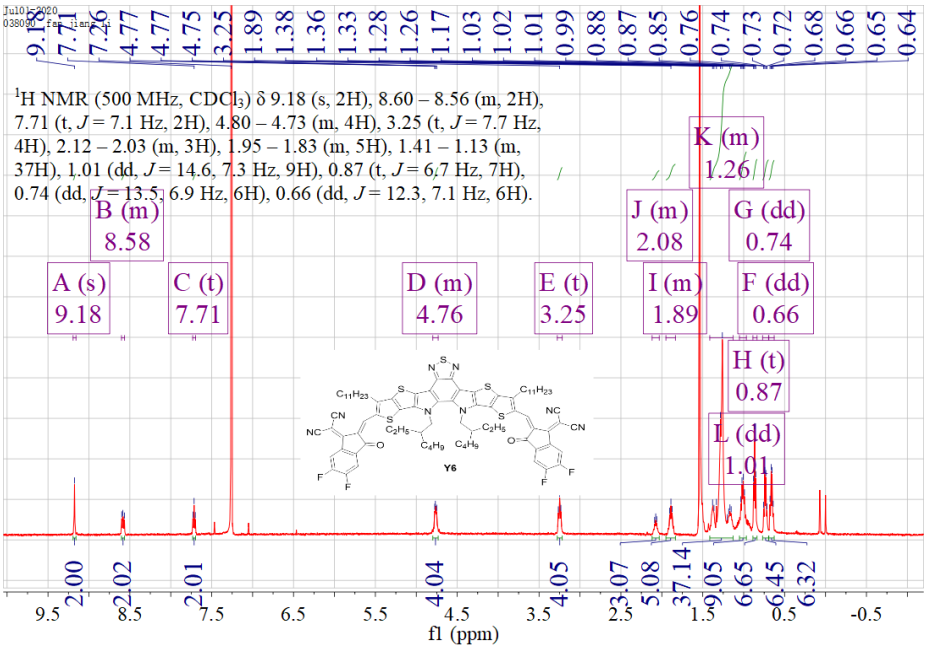

Figure S1 ^{1}H NMR spectra of IR-Y6 in $CDCl_3$.

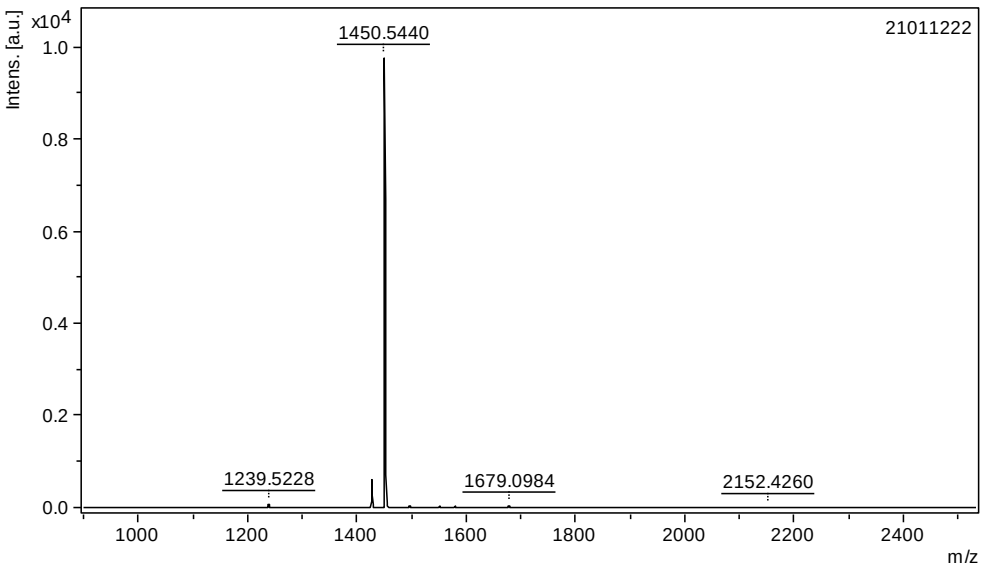

Figure S2 The mass spectra (MALDI-TOF) of IR-Y6.

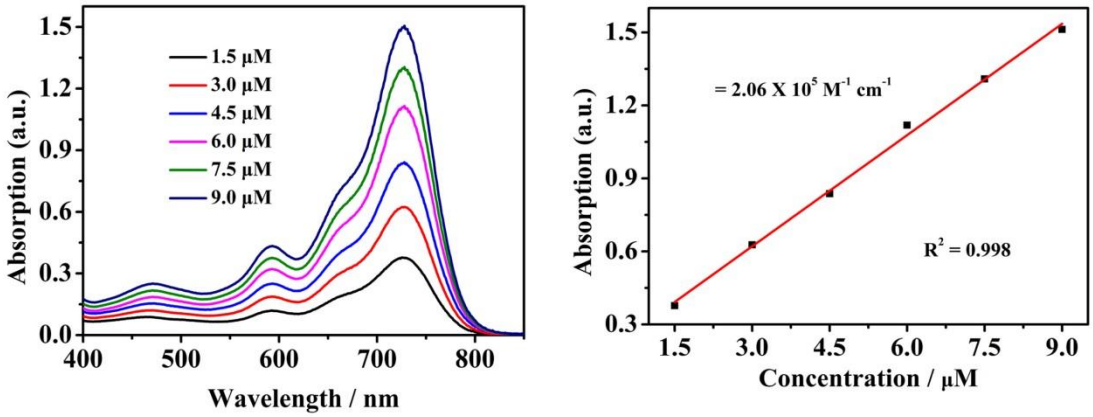

Figure S3 The absorption spectra of IR-Y6 in $CHCl_3$ with different concentrations.

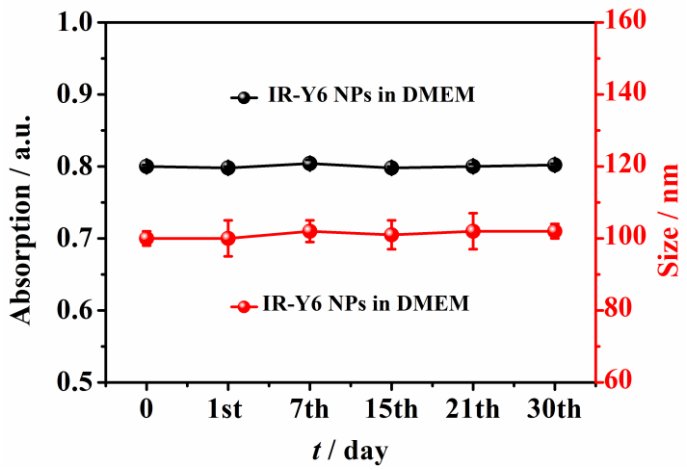

Figure S4 The optical stability and chemical stability of IR-Y6 NPs in DMEM.

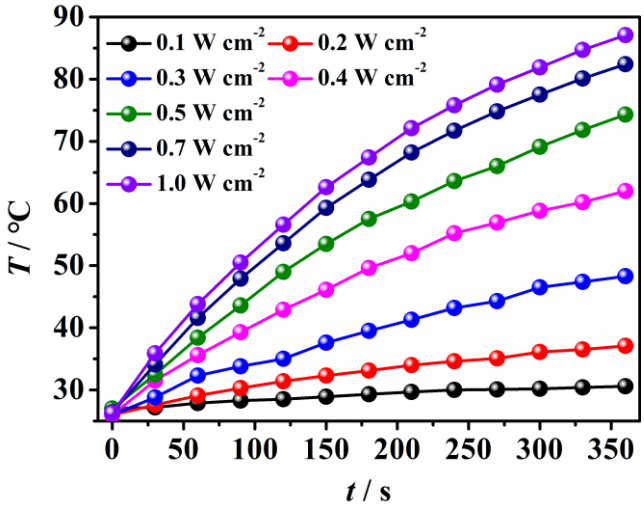

Figure S5 Photothermal curves of IR-Y6 NPs (30 μg mL^{-1}) under different laser power densities

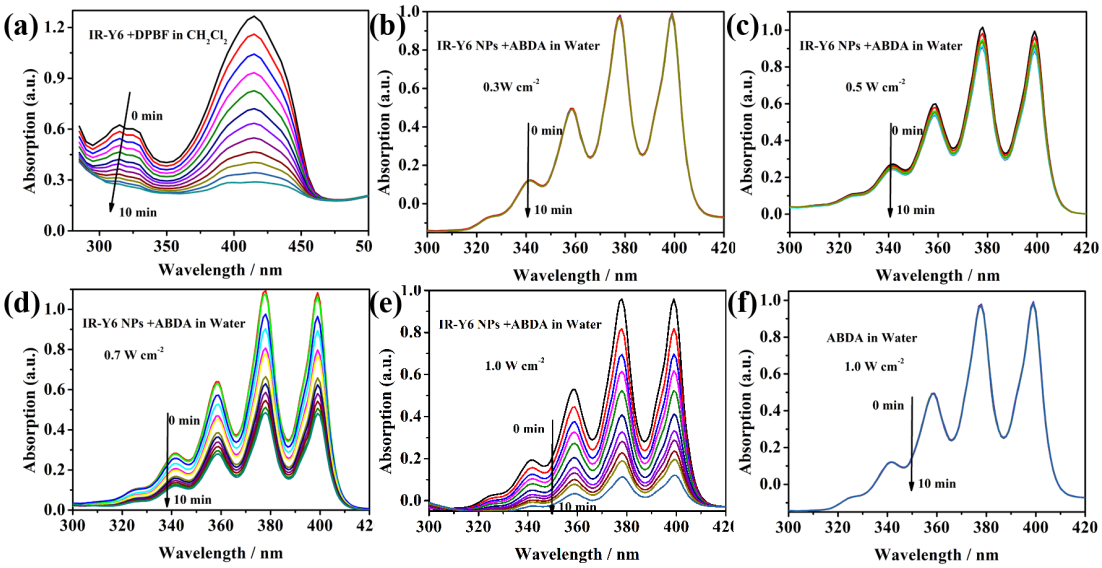

Figure S6 Absorption spectra of IR-Y6 in CH_2Cl_2 mixed with DPBF (a) and IR-Y6 NPs in PBS mixed with ABDA (b, c, d, e, f) under 808 nm laser with different power densities.

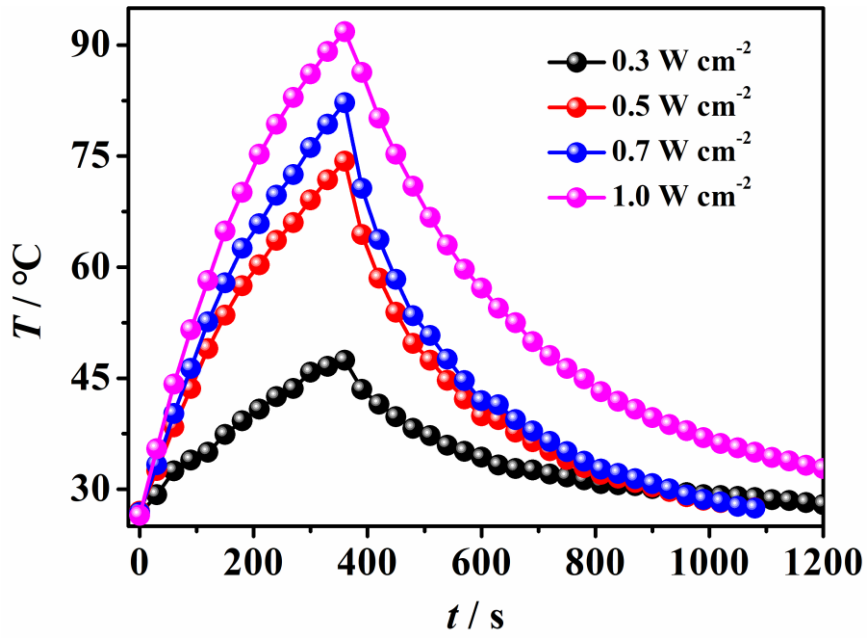

Figure S7 Photothermal effect of IR-Y6 NPs (30 μg mL^{-1}) in water under different laser irradiation.

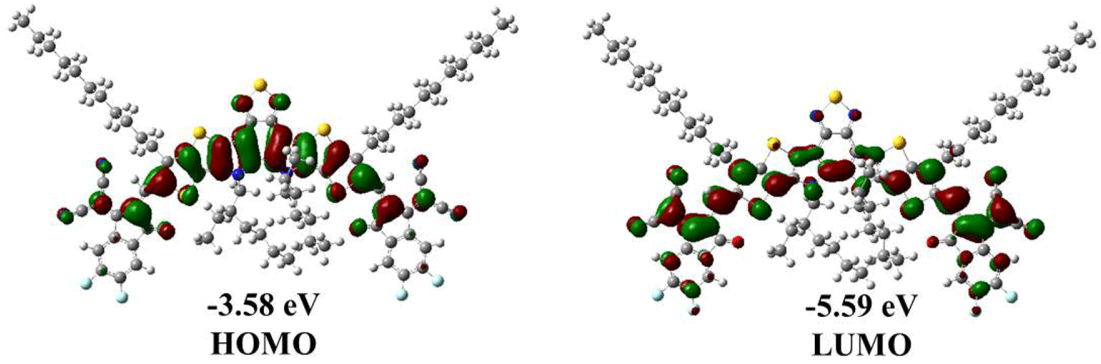

Figure S8 HOMO and LUMO of IR-Y6.

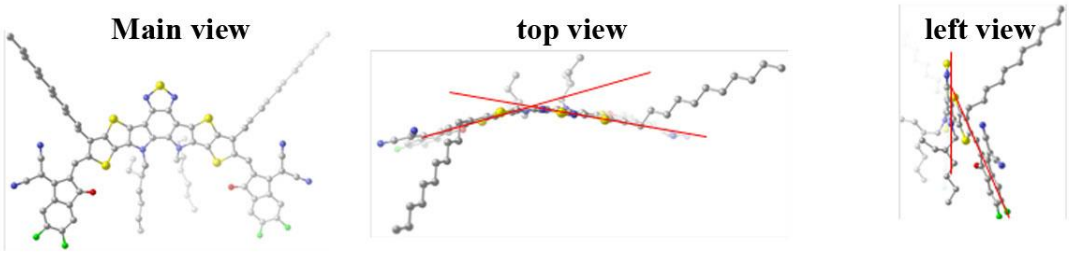

Figure S9 The optimization geometries of IR-Y6.

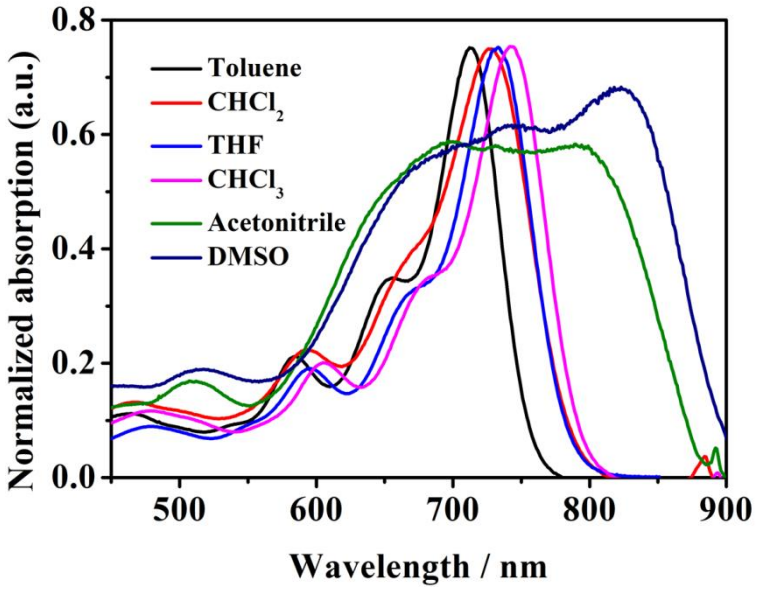

Figure S10 Normalized absorption spectra of IR-Y6 in different polar solvents: toluene < dichloromethane (CH_2Cl_2) < tetrahydrofuran (THF) < trichloromethane ($CHCl_3$) < Acetonitrile < DMSO.

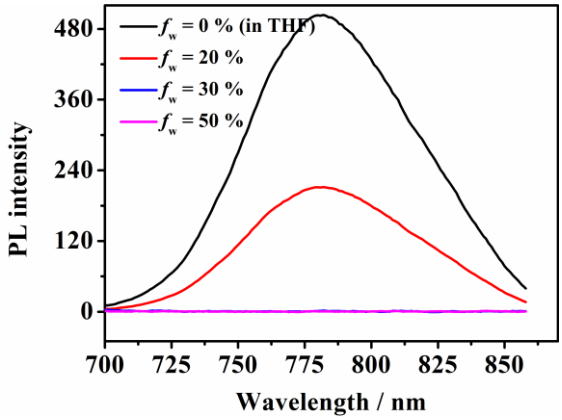

Figure S11 PL spectra of the IR-Y6 in THF/water mixtures with different water fractions

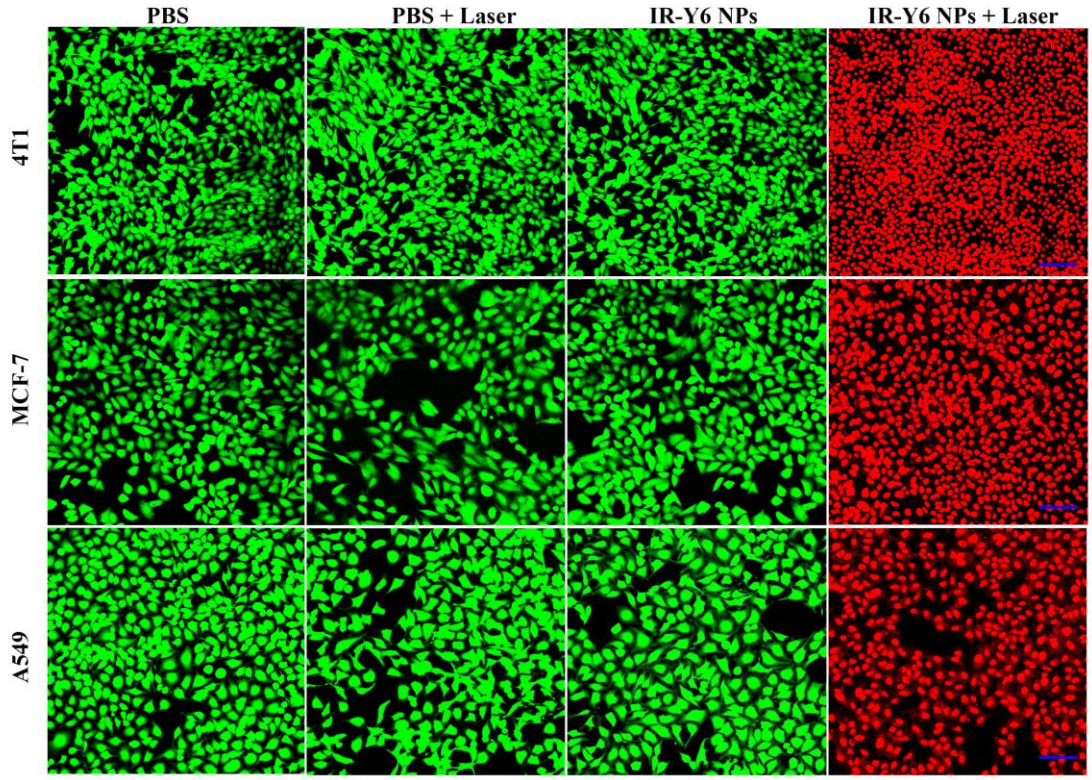

Figure S12 Calcein AM (green)/propidium iodide (red) co-staining fluorescence imaging of 4T1, MCF-7, and A549 cells after same treatments with IR-Y6 NPs (30 μg mL^{-1}) and NIR irradiation. NIR laser: 808 nm, laser power: 0.5 W cm^{-2}, irradiation time: 6 min. Scale bar: 100 μm.

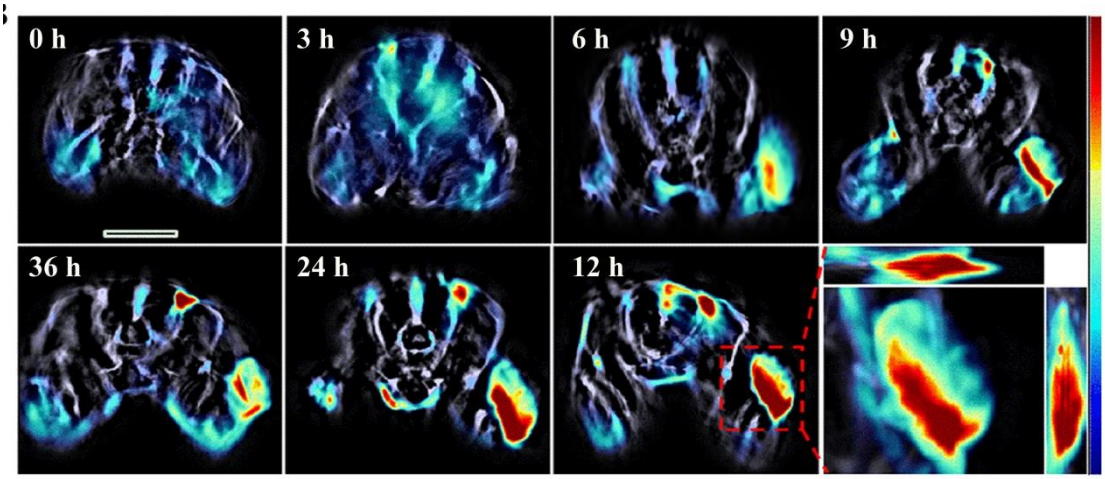

Figure S13 Real-time PAI of mice after systemic administration of IR-Y6 NPs (150 μL, 1 mg mL^{-1}) through intravenous injection.

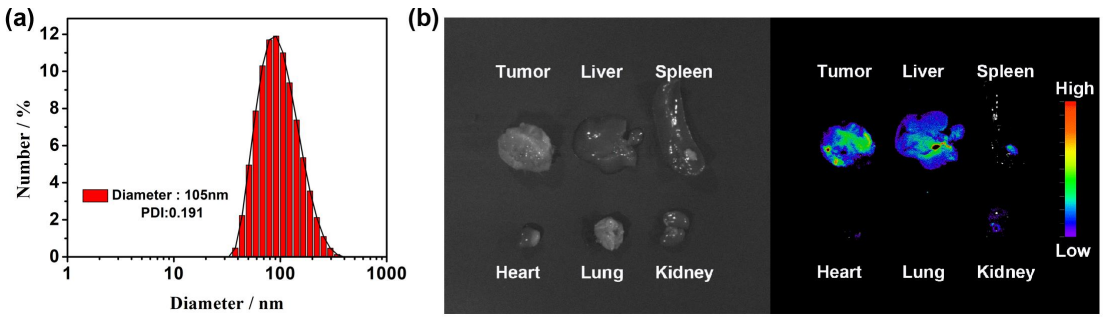

Figure S14 (a) DLS of IR-Y6&FITC NPs. (b) Fluorescence imaging of major isolated organs and tumor

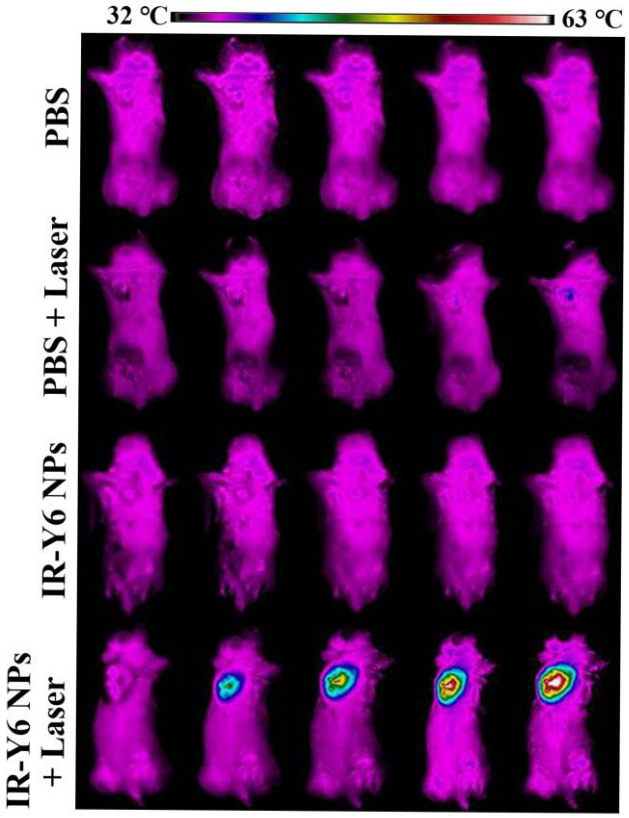

Figure S15 Infrared thermal images of 4T1-tumor-bearing nude mice after various treatments.

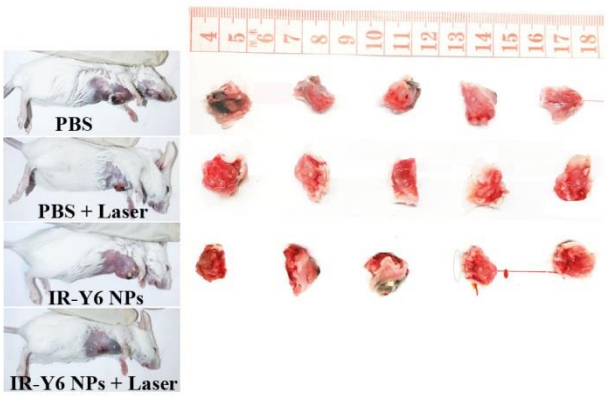

Figure S16 Tumor photographs of mice at day 21 after various treatments.

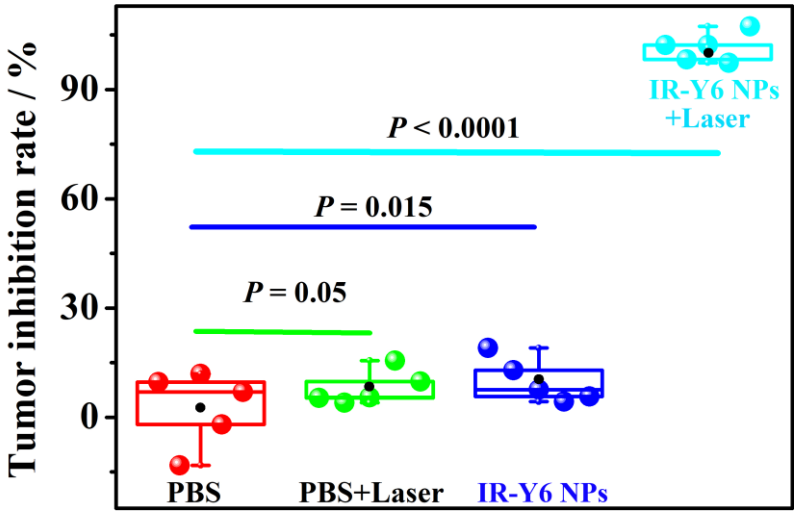

Figure S17 Tumor suppression efficacy of different treatments.

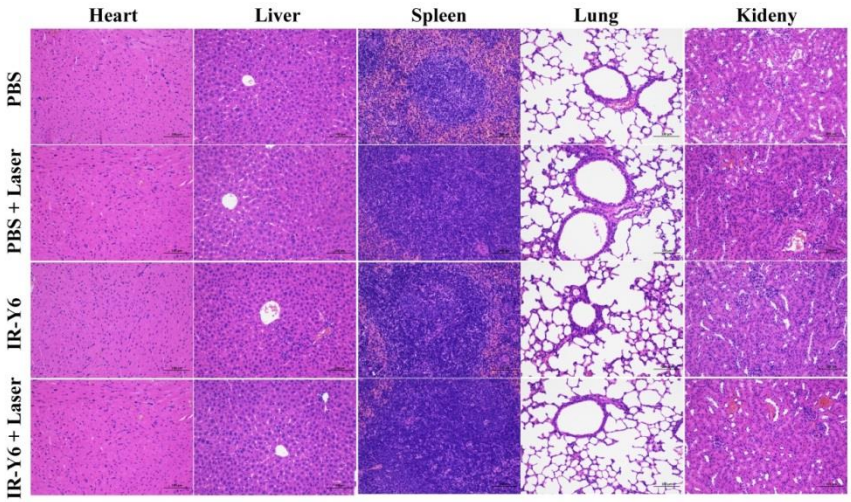

Figure S18 H&E staining of the major organs dissected from mice at day 21 after various treatments. Scale bar: 200 μm.

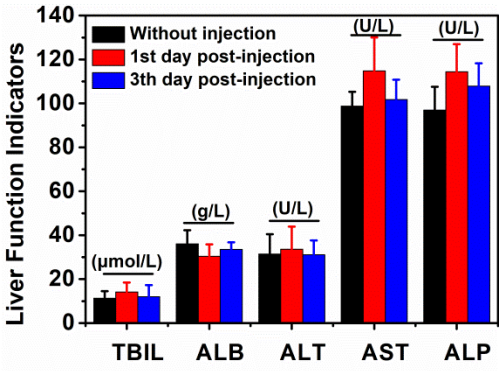

Figure S19 Hematological assessment of liver function indicators of mice treated without injectio n of IR-Y6 NPs, treated with IR-Y6 NPs on the first day post-injection, and on the third day post-injection, respectively.

Table S1 Test report of blood cells analyzer

Parameters	without injection	1st day post-injection	3th day post-injection	Reference	unit
WBC	1.5	5.2	1.5	0.8-6.8	10^9/L
Lymph	1.2	3.4	0.9	0.7-5.7	10^9/L
Mon	0	0.1	0	0.0-0.3	10^9/L
Gran	0.3	0.5	0.6	0.1-1.8	10^9/L
Lymph	79.8	83.4	78.1	55.8-90.6	%
Mon	2.2	4.2	2.3	1.8-6.0	%
Gran	18.4	25.2	37.1	8.6-38.9	%
RBC	8.19	8.02	7.79	6.36-9.42	10^12/L
HGB	120	125	114	110-143	g/L
HCT	39.8	38.7	37.9	34.6-44.6	%
MCV	48.7	48.3	48.7	48.2-58.3	fL
MCH	14.6	15.5	14.6	15.8-19	pg
MCHC	301	322	300	302-353	g/L
RDW	13.2	13.1	13.4	13-17	%
PLT	464	838	503	450-1590	10^9/L
MPV	5.3	5.2	4.9	3.8-6.0	fL

Synthesis and Characterization of target oligomers. IR-Y6 was synthesized via a Knoevenagel condensation reaction according to the previously reported method ^{1}H NMR (Bruker AVANCE III 500 MHz, $CDCl_3$) δ: 9.18 (s, 2H), 8.60- 8.56 (m, 2H), 7.71 (t, J = 7.1 Hz, 2H), 4.80-4.73 (m, 4H), 3.25 (t, J = 7.7 Hz, 4H), 2.12-2.03 (m, 3H), 1.95-1.83 (m, 5H), 1.41-1.13 (m, 37H), 1.01 (dd, J = 14.6, 7.3 Hz, 9H), 0.87 (t, J = 6.7 Hz, 7H), 0.74 (dd, J = 13.5, 6.9 Hz, 6H), 0.66 (dd, J = 12.3, 7.1 Hz, 6H). High-resolution mass spectra (MALDI-TOF MASS) calculated m/z for [$C_{82}H_{86}F_4N_8O_2S_5$] calculated 1450.544, found (m/z): 1450.5440.

Methods

^{1}H-NMR spectra of compounds was performed with Bruker Avance Ⅲ 400/500 spectrometer. Mass spectrometric (MS) data were carried out using Waters MALDI micro MX, America. Absorption and emission spectra were performed with a Lambda UV-visible spectrophotometer (PerkinElmer) and a VAEIAN CARY Eclipse fluorescence spectrophotometer (Serial No. FL0812-M018), respectively. Steady-state fluorescence spectra and time-resolved luminescence spectra were recorded on a fluorometer named Cary Eclipse from Agilent Tech. Data were obtained under the control of a Windows-based PC by running the manufacturers' supplied software. Nanosecond fluorescence lifetimes were performed using the TCSPC technique on HORIBA Jobin Yvon IBN photo counting fluorescence system with nano LED laser excitation at 455 nm, and microsecond fluorescence lifetimes were performed using spectra LED laser excitation at 460 nm. The molecular geometries calculations, including density functional theory and potential energy curves, were done with the Gaussian 09 suite. The molecular dynamic (MD) simulation was performed using Gromacs (Version 5.1.4) package. Confocal laser scanning microscope (CLSM) images were performed on Olympus FV3000 confocal laser scanning microscope. Photoacoustic imaging was carried out by the InVision 128 MSOT system (iTheraMedical, Germany). A laser at λ = 808 nm was employed as the light source for in vitro and in vivo experiments. The output power of the laser was controlled by a fiber coupled laser system (FCW-808-30W, Changchun New Industries

Optoelectronics Technology) and measured by a power meter (CEL-NP2000, Beijing Zhongjiao Jinyuan Technology Co., Ltd.). The temperature changes were monitored by FLIR-1910582 thermal camera.

The imaging of IR-Y6 NPs distribution in the main organs of mice

In order to more intuitively observe the distribution of nanoparticles in the main organs of mice, IR-Y6 and FITC (mass fraction of 10:1) were simultaneously prepared into nanoparticles (IR-Y6&FITC NPs) by DSPE-PEG2000 as encapsulating material. Fluorescein isothiocyanate (FITC) has been widely used for its excellent photoluminescence properties. Its maximum absorption wavelength is 490~495 nm, and the maximum emission wavelength is 525~530 nm. IR-Y6&FITC NPs has both optical absorption properties and fluorescence properties of FITC with maximum emission of 525~530 nm. 4T1-Tumor-bearing mice was injected IR-Y6&FITC NPs NPs (150 μL, 1 mg mL^{-1}), after 12 h injection, all the mice were euthanized and their major organs and tumor were dissected and imaged by using Living Imaging System (LB983 NC100).

Photothermal conversion efficiency calculation

The photothermal conversion efficiencies (η) were measured according to the reported method:

$$\eta = \frac{hs(T_{Max} - T_{Surr}) - Q_{Dis}}{I(1 - 10^{-A808})} \quad \textbf{(S1)}$$

h is the heat transfer coefficient; s is the surface area of the container. Q_{Dis} represents heat dissipated from the laser mediated by the solvent and container. I is the laser power and A is the absorbance at 808 nm.

$$hs = \frac{mC_{water}}{\tau} \quad \textbf{(S2)}$$

m is the mass of the solution containing the photoactive material, C is the specific heat capacity of the solution (C_{water} = 4.2 J/(g•°C)), and τ is the associated time constant.

$$t = -\tau \ln\theta \quad \textbf{(S3)}$$

θ is a dimensionless parameter, known as the driving force temperature

$$\boldsymbol{\theta = \frac{T - T_{Surr}}{T_{Max} - T_{Surr}}} \qquad \textbf{(S4)}$$

T_{max} and T_{Surr} are the maximum steady state temperature and the environmental temperature, respectively.